

Functionalized few-layer silicene nanosheets: density functional theory on stability, structural, and electronic properties

Bruno Ipaves,[†] João F. Justo,[‡] and Lucy V. C. Assali^{*,†}

[†]*Instituto de Física, Universidade de São Paulo,
CEP 05508-090, São Paulo - SP, Brazil*

[‡]*Escola Politécnica, Universidade de São Paulo,
CEP 05508-010, São Paulo - SP, Brazil*

E-mail: ipaves@if.usp.br, jjusto@lme.usp.br, lassali@if.usp.br

Abstract

Using density functional theory calculations, we investigated the properties of few-layer silicene nanosheets, namely bilayers and trilayers, functionalized with group-III or group-V atoms of the periodic table. We considered the Si_2X_2 bilayers and the Si_2X_4 trilayers, $\text{X} = \text{B}, \text{N}, \text{Al}, \text{P}$. We computed the structural, energetic, dynamic, elastic, and electronic properties of those systems in several stacking configurations, labeled as AA' , AB , $\text{AA}'\text{A}''$, and ABC . The results revealed that $\text{AA}'\text{-Si}_2\text{N}_2$, $\text{AB-Si}_2\text{N}_2$, $\text{AA}'\text{-Si}_2\text{P}_2$, $\text{AB-Si}_2\text{P}_2$, $\text{ABC-Si}_4\text{B}_2$, $\text{ABC-Si}_4\text{Al}_2$, $\text{AA}'\text{A}''\text{-Si}_4\text{P}_2$, and $\text{ABC-Si}_4\text{P}_2$ nanosheets are all dynamically stable, according to their respective phonon dispersion spectra. Additionally, by comparing the standard enthalpies of formation of doped few-layer silicene systems with the ones of the pristine silicene monolayer, bilayer, and trilayer nanosheets, we found that those structures could be experimentally accessed. Exploring the electronic properties of those stable systems, we discovered that the

silicene bilayers and trilayers functionalized with N or P atoms change from a metallic to a semiconducting behavior. However, the metallic behavior is kept when the nanosheets are functionalized with B or Al atoms. Finally, by placing our results within the context of silicon-based systems previous investigations, we could envision potential applications for those nanosheets in van der Waals heterostructures, alkali-metal ion batteries, UV-light devices, and thermoelectric materials.

Introduction

Since the discovery and isolation of graphene sheets,¹ several 2D materials have been reported in the literature with different physical properties, with metallic (NbSe₂), insulating (hBN), and semiconducting (MoS₂) behaviors.^{2,3} Due to their remarkable properties, those 2D materials have been considered for applications in many areas, such as in electronics, medicine, energy generation and storage, light processing, and sensors and actuators.

Silicene, a 2D hexagonal silicon monolayer, presents some properties analogous to those of graphene, including the honeycomb structure with Dirac cone at the high-symmetry K-point in the first Brillouin zone.⁴⁻⁶ Hence, it has been considered a promising candidate to be used in similar applications like those of graphene.⁷ Unlike graphene, silicene is not a flat nanosheet due to the silicon sp^2 - sp^3 hybridizations, resulting in a low-buckled structure.^{5,6,8} This buckling makes silicene very reactive to hydrogenation, fluorination, and doping with substitutional atoms, which modify substantially its properties and may transform it from a zero band gap semimetal into a metallic or semiconducting material.^{9,10} Although silicene monolayer has been intensively studied, systems involving few-layer silicene (FLS) systems have received less attention over the last few years.¹¹ However, it is considerably easier to synthesize FLS than the silicene monolayer.¹² Furthermore, FLS properties are highly dependent on the stacking order and interlayer interactions, e.g., the silicene bilayer could have metallic or semiconducting behavior by simply changing its morphology,^{13,14} a feature that is very attractive from a technological perspective.

Free-standing FLS nanosheets have been synthesized by liquid oxidation and exfoliation of CaSi₂ and three possible stacking configurations have been proposed: AA, AABB, and ABC.¹⁵ There are recent studies of silicon-based binary compounds, such as Si₂X₂ (X = N, P, As, Sb, or Bi)¹⁶ and Si₂XY (X, Y = P, As, Sb, or Bi), which exhibit a variety of properties.¹⁷ These 2D binary systems are structurally similar to the silicene bilayer since they are composed of two silicene sheets 50% doped with substitutional atoms, as Si-Si bonds between neighboring layers are covalent. The 2D silicon-based materials have potential

applications in several fields, such as anodes in lithium-ion batteries (LIBs),¹⁵ spintronics,¹⁷ optoelectronic and electronic devices,¹⁸ energy storage,¹⁹ and field-effect transistor pressure sensors.²⁰

Considering the potential applications of FLS nanosheets, it is of great interest to understand the properties of these materials in several functionalized structures. Here, we performed a theoretical investigation on the physical properties of silicene bilayers and trilayers functionalized with group-III (B and Al) and group-V (N and P) atoms of the periodic table in a variety of stacking configurations, using the density functional theory and the supercell approach. We computed the structural and electronic properties of pure FLS and the changes resulting from such functionalizations. Then, we determined the dynamic stability, enthalpy of formation, and elastic constants of those structures.

We labeled the functionalized silicene bilayers and trilayers respectively as Si_2X_2 and Si_4X_2 ($\text{X} = \text{B}, \text{N}, \text{Al}, \text{P}$). The bilayers consist of two 50% X-doped silicene nanosheets and the trilayers consist of three silicene nanosheets, one non-doped silicene layer between two 50% X-doped ones. Herein, we considered four stacking configurations: AA' and AB for bilayers; and $\text{AA}'\text{A}''$ and ABC for trilayers, with Si-Si covalent bonds. We found that the Si_2B_2 and Si_2Al_2 bilayers, and the $\text{AA}'\text{A}''-\text{Si}_4\text{N}_2$, $\text{ABC}-\text{Si}_4\text{N}_2$, $\text{AA}'\text{A}''-\text{Si}_4\text{B}_2$, and $\text{AA}'\text{A}''-\text{Si}_4\text{Al}_2$ trilayers are not dynamically stable. We explored in depth the physical properties of dynamically stable nanosheets, that can be classified in two distinct groups according to their band structure: (i) the metallic $\text{ABC}-\text{Si}_4\text{B}_2$ and $\text{ABC}-\text{Si}_4\text{Al}_2$ trilayers; (ii) the indirect band gap semiconductors Si_2N_2 and Si_2P_2 bilayers in both AA' and AB stacking configurations, as well as the Si_4P_2 trilayer in both $\text{AA}'\text{A}''$ and ABC stacking arrangements.

Regarding the dynamically stable systems, they present enthalpies of formation lower than that of pristine silicene and, hence, they could be synthesized easily. Particularly, we found that the indirect band gap semiconductors are the most promising systems to be produced as free-standing 2D materials. Finally, based on our results combined with the ones from previous works that studied similar structures, we suggest that these stable systems

could be explored for van der Waals heterostructures, alkali-metal ion batteries (AMIBs), UV-light devices, and thermoelectric materials applications.

The paper is organized as follows: first, we present the theoretical methodology and computational details, then the results on energetic, structural, stability, and electronic properties are presented. The last section presents a discussion and concluding remarks.

Theoretical Model and Computational Details

All calculations were performed using the Quantum ESPRESSO computational package^{21,22} with the electronic interactions described within the density functional theory^{23,24} (DFT) and the wave functions were expanded with the projector augmented wave (PAW) method.²⁵ We used the generalized gradient approximation of Perdew-Burk-Ernzerhof (PBE) for the exchange and correlation potential,²⁶ augmented by the dispersive van der Waals interaction within the Dion *et al.* scheme²⁷ and optimized by Klimeš *et al.* (optB88-vdW).²⁸ Those approximations have been used by recent investigations, which have shown the relevance of describing the vdW interactions appropriately, particularly when treating the vibrational properties of the systems.²⁹⁻³¹

An 1100 eV energy cutoff for the valence electrons plane wave expansion was used and self-consistent iterations were performed until reaching convergence in total energies of 0.1 meV/atom. During structural optimization, relaxations and distortions were considered in all ions, without symmetry constraints, until forces in any ion were lower than 1 meV/Å. The irreducible Brillouin zones (BZ) for computing the electronic states were sampled by a $16 \times 16 \times 1$ Monkhorst-Pack k -point grid.³²

The 2D structures were built with a hexagonal simulation supercell, considering periodic boundary conditions. A lattice parameter of 25 Å was used in the perpendicular direction to the sheets (z -axis) to prevent interactions among cell images. The primitive cells contained 4 and 6 atoms, respectively, for the bilayers and trilayers. The cell parameters in the xy

plane were obtained using a variable-cell optimization, and the respective phonon dispersion curves were obtained through the density functional perturbation theory (DFPT),³³ with the irreducible Brillouin zones sampled by an $8 \times 8 \times 1$ q -point mesh.

To determine the elastic properties of the systems, we built a rectangular cell with 8 atoms for the bilayers and 12 atoms for the trilayers. The elastic constants were evaluated with the strain–energy method, by applying two in-plane strains (ϵ), ranging from -1.5% to 1.5% with respect to the optimized cell parameters: (i) uniaxial deformation along the zigzag direction and (ii) biaxial planar deformation (zigzag and armchair simultaneously).³⁴ The elastic energy is expressed by

$$E(\epsilon) = E(0) + \frac{1}{2}U^{(2)}\epsilon^2 + O(\epsilon^3), \quad (1)$$

where $E(\epsilon)$ and $E(0)$ are the total energies of strained and unstrained configurations, respectively. For isotropic structures, $U^{(2)}$ is the C_{11} elastic constant for zigzag axial deformation, whereas it is $2(C_{11} + C_{12})$ for biaxial planar deformation.³⁴ Accordingly, the relevant elastic constants were obtained by fitting a second-order polynomial to the data.

The standard enthalpy of formation ΔH_f^0 , per atom and at zero temperature, of each structure was computed by

$$\Delta H_f^0 = \frac{E_t(\text{Si}_y\text{X}_2) - yE_t(\text{Si}) - 2E_t(\text{X})}{y + 2}, \quad (2)$$

where $E_t(\text{Si}_y\text{X}_2)$ is the total energy of the 2D system, with y Si atoms and 2 X atoms ($X = \text{B}, \text{N}, \text{Al}, \text{P}$), y being 2 and 4 for bilayers and trilayers, respectively. Since the standard enthalpy of formation is a measurement of the energy released or absorbed when a substance is synthesized from its pure elements, the $E_t(\text{Si})$ and $E_t(\text{X})$ are the total energies, per atom, of the respective Si and X standard states. Those energies, computed within the same methodology previously described, were obtained from the total energy of crystalline silicon in a diamond lattice, boron in a trigonal crystalline structure (β -boron), aluminum in a

face-centered cubic crystalline structure, nitrogen in an isolated N_2 molecule, and bulk black phosphorus. This procedure to determine enthalpies and/or energies of formation has been successfully used to investigate several other systems.^{35–37}

Physical Properties of Functionalized FLS Nanosheets

Structural properties

Figure 1 shows schematic representations of the Si_2X_2 bilayers, in the AA' and AB stacking arrangements, and Si_4X_2 trilayers, in the AA'A'' (or AA'A) and ABC stacking configurations, with $X = B, N, Al, P$. Moreover, when $X = Si$ in the figure, it indicates pristine silicene monolayer Si_2 , bilayer Si_4 , and trilayer Si_6 , which received those labels due to the number of Si atoms in the simulation unit cell. The figure also exhibits the labels given to the intralayer (d), interlayer (h), and buckling (Δz) distances, as well as the intraplanar bond angle (θ).

Table 1 presents the optimized structural parameters of the Si_2X_2 bilayers and Si_4X_2 trilayers, as well as the respective values obtained for pristine silicene Si_2 monolayer, Si_4 bilayers, and Si_6 trilayers, where the distance labels are consistent with the ones defined in figure 1. The table also displays the respective standard enthalpy of formation ΔH_f^0 and the dynamic stability (DS).

Starting with the pristine FLS, we found that the lattice constants for all of nanosystems are very close, ranging from 3.847 Å (AB– Si_4) to 3.870 Å (Si_2). On the other hand, the calculated buckling distances in the Si_4 and Si_6 layers, despite having similar values, are on the order of 43% larger than the value of 0.482 Å found in pure silicene Si_2 monolayer. Additionally, Si_2 has an intraplanar bond angle θ of 115.67°, which is related to sp^2 - sp^3 hybridization, while the θ values, obtained for AA'A– Si_6 and ABC– Si_6 trilayers, are 111.62° and 111.51°, respectively, which are closer to the sp^3 hybridization angle value of 109.47°. As the number of layers increases, the θ values decrease towards the tetrahedral value, as Si atoms prefer the sp^3 hybridization.^{38,39} Moreover, unlike the few-layer graphene and graphite, which present weak interlayer van der Waals interactions, in the FLS the layers

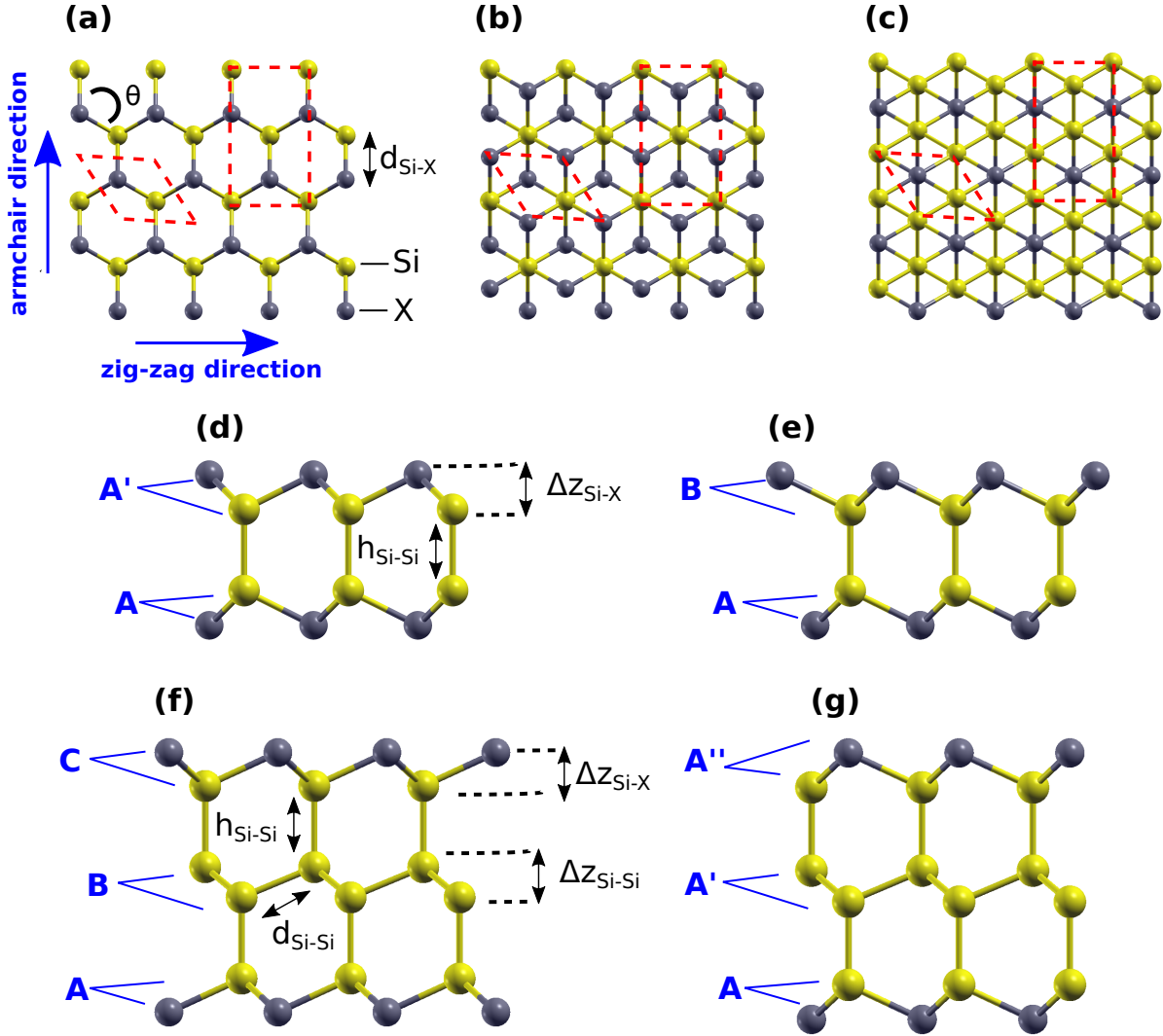


Figure 1: Schematic representations of the Si_2X_2 bilayers and Si_4X_2 trilayers ($X = \text{B}, \text{N}, \text{Al}, \text{P}$) structures. Herein, $X = \text{Si}$ means pristine silicene bilayer (Si_4) and trilayer (Si_6). Top view perspective of (a) AA' and $\text{AA}'\text{A}''$, (b) AB , and (c) ABC stacking configurations; and side view perspective of (d) AA' , (e) AB , (f) ABC , and (g) $\text{AA}'\text{A}''$ stacking configurations. The $\text{AA}'\text{A}''$ stacking is also known as $\text{AA}'\text{A}$ in pure silicene trilayer. The yellow and gray spheres represent respectively Si and X atoms. The red dashed lines represent the unit cell limits, hexagonal (rectangle) cells used to determine dynamic, structural, and electronic (elastic) properties. These schemes also indicate the labels given to the $d_{\text{Si-Si}}$ and $d_{\text{Si-X}}$ intralayer, $h_{\text{Si-Si}}$ interlayer, $\Delta z_{\text{Si-Si}}$ and $\Delta z_{\text{Si-X}}$ buckling distances, and the θ intraplanar bond angle.

Table 1: Structural properties of Si_2X_2 bilayers and Si_4X_2 trilayers ($\text{X} = \text{B}, \text{N}, \text{Al}, \text{P}$): lattice parameters (a), intralayer (d), interlayer (h), and buckling (Δz) distances, given in Å, and the intraplanar bond angle (θ), labeled according to figure 1. The standard enthalpy of formation (ΔH_f^0), obtained according to equation 2, is given in meV/atom. For pristine silicene Si_2 monolayer, Si_4 bilayers, and Si_6 trilayers, $\text{X} = \text{Si}$. The last column indicates the dynamic stability (DS) of the structures.

Structural parameters											
System	Structure	Stacking	a	$d_{\text{Si-X}}$	$h_{\text{Si-Si}}$	$d_{\text{Si-Si}}$	$\Delta z_{\text{Si-X}}$	$\Delta z_{\text{Si-Si}}$	θ	ΔH_f^0	DS
Monolayer	Si_2	—	3.870	2.285	—	—	0.482	—	115.67	751	Yes
	Si_4	AA'	3.854	2.325	2.470	—	0.676	—	111.89	609	Yes
AB		3.847	2.322	2.538	—	0.676	—	111.89	570	Yes	
Bilayer	Si_2B_2	AA'	3.448	1.993	2.565	—	0.109	—	119.70	648	No
		AB	3.468	2.005	2.498	—	0.104	—	119.73	704	No
	Si_2Al_2	AA'	4.231	2.457	2.572	—	0.271	—	118.79	446	No
		AB	4.242	2.457	2.514	—	0.200	—	119.34	404	No
	Si_2N_2	AA'	2.909	1.767	2.429	—	0.548	—	110.81	-743	Yes
		AB	2.921	1.771	2.393	—	0.541	—	111.08	-733	Yes
	Si_2P_2	AA'	3.544	2.286	2.380	—	1.019	—	101.65	-87	Yes
		AB	3.557	2.287	2.351	—	1.007	—	102.06	-84	Yes
Trilayer	Si_6	AA'A	3.858	2.332	2.423	2.355	0.690	0.756	111.62	224	Yes
		ABC	3.858	2.333	2.435	2.355	0.695	0.764	111.51	220	Yes
	Si_4B_2	AA'A''	3.539	2.045	2.495	2.282	0.092	1.019	119.79	552	No
		ABC	3.568	2.061	2.403	2.272	0.086	0.900	119.82	529	Yes
	Si_4Al_2	AA'A''	4.128	2.390	2.439	2.515	0.175	0.802	119.46	339	No
		ABC	4.143	2.399	2.419	2.516	0.185	0.782	119.40	309	Yes
	Si_4N_2	AA'A''	2.911	1.763	2.384	2.508	0.533	1.861	111.27	-156	No
		ABC	2.865	1.751	2.433	2.807	0.574	2.267	109.78	-188	No
	Si_4P_2	AA'A''	3.641	2.321	2.365	2.283	0.984	0.890	103.32	-6	Yes
		ABC	3.665	2.330	2.356	2.292	0.974	0.880	103.74	-7	Yes

are covalently bonded. Accordingly, the interlayer $h_{\text{Si-Si}}$ distances are in the 2.423-2.538 Å range, the smallest one associated with the trilayers, all values close to the interatomic distance of crystalline silicon (2.352 Å). Those results are in good agreement with the ones reported in the literature.^{11,13,38,40}

According to table 1, when the silicene bilayer is 50% doped with substitutional B, Al, or P atoms, the lattice parameter a changes by about 10%, decreasing in the Si_2B_2 and Si_2P_2 bilayers, and increasing in the Si_2Al_2 ones, regardless of the stacking configuration. In contrast, the N atom substitution considerably affects the a value, i.e., the lattice parameter decreases $\approx 25\%$ in both Si_2N_2 stacking configurations. Therefore, while the Al substitution stretched out the lattice parameter a and the intralayer distance $d_{\text{Si-Al}}$, in comparison with pristine silicene bilayers, the incorporation of B, N, or P atoms reduced them. The values $d_{\text{Si-Al}} = 2.457$ Å and $d_{\text{Si-B}} \approx 2.0$ Å for, respectively, Si_2Al_2 and Si_2B_2 bilayers are close to the ones reported by Ding *et al.*¹⁰ in the Al/B doped silicene monolayer: 2.42 Å for SiAl, 2.43 Å for AlSi₃, 1.96 Å for SiB, and 1.94 Å for BSi₃.

It can be noticed that in the bilayer systems functionalized with group-III atoms (B and Al, with valence electronic configuration ns^2np^1 , $n = 2$ and 3, respectively), the intraplanar bond angles are greater than in the pristine Si_4 bilayer, being very close to the value of 120° , which is the expected value of the sp^2 -type hybridization of B and Al atoms bonded to three adjacent Si atoms. Consequently, the buckling distances are greatly affected by the substitution, being reduced by about 85% in the Si_2B_2 bilayer for both stacking configurations ($\Delta z_{\text{Si-B}} \approx 0.11$ Å), by about 60% in the $\text{AA}'\text{-Si}_2\text{Al}_2$ bilayer ($\Delta z_{\text{Si-Al}} \approx 0.27$ Å), and by about 70% in the $\text{AB-Si}_2\text{Al}_2$ bilayer ($\Delta z_{\text{Si-Al}} \approx 0.20$ Å).

On the other hand, in the bilayer systems functionalized with group-V atoms (N and P, with valence electronic configuration ns^2np^3 , $n = 2$ and 3, respectively), according to table 1, the intraplanar bond angles are smaller than in the pristine Si_4 sheet, approaching the sp^3 -type hybridization angle value, with three bonds and a lone pair. Those values are a little greater than 109.47° for the Si_2N_2 systems while they are smaller than that value for

the Si_2P_2 nanosheets. The P atom substitution causes major modifications in the pristine buckling distances as $\Delta z_{\text{Si-P}} \approx 1.0 \text{ \AA}$ in the Si_2P_2 bilayer, for both stacking configurations, whilst for the N atom substitution the buckling distances are $\Delta z_{\text{Si-N}} \approx 0.5 \text{ \AA}$, a value that is in the range between the ones found for pristine silicene monolayer and bilayers. The functionalized bilayers present interlayer distances $h_{\text{Si-Si}}$ slightly greater/smaller than the ones of pristine silicene bilayers, indicating that the strong Si-Si covalent bonds are maintained. Moreover, the structural parameters of Si_2N_2 and Si_2P_2 systems agree with the available reported data.¹⁶

The pristine silicene Si_6 trilayers have lattice parameters a of 3.858 \AA and present additional structural parameters in comparison to the bilayer systems, namely, the intralayer $d_{\text{Si-Si}}$ and buckling $\Delta z_{\text{Si-Si}}$ distances. The $d_{\text{Si-Si}} = 2.355 \text{ \AA}$ obtained for both stacking configurations, as well as the $\Delta z_{\text{Si-Si}}$ of 0.756 \AA and 0.764 \AA , found in the AA'A and ABC stacking configurations, are very close to the Si bulk values of 2.352 \AA and 0.784 \AA for $d_{\text{Si-Si}}$ and $\Delta z_{\text{Si-Si}}$, respectively.

The B, Al, or P doping of Si_6 modify the lattice parameter by about 7%, which increases in the Si_4Al_2 sheets and decreases in the Si_4B_2 and Si_4P_2 ones, irrespective of the stacking configuration. The Si_4P_2 structures exhibit the closest lattice parameters to the one of pure silicene trilayers, in which we found lattice parameters a of 3.641 and 3.665 \AA for AA'A'' and ABC stacking configurations, respectively. Nevertheless, the presence of N affects substantially the a values, decreasing them by more than 25%, as compared to that of the pristine systems, in both Si_4N_2 stacking configurations. Those systems present the smallest lattice parameters among all trilayers studied here, consistent with the Si_2N_2 systems among the bilayers.

The Si_4Al_2 trilayers present lattice parameters a of about 4.1 \AA , with buckling distances $\Delta z_{\text{Si-Al}}$ and intraplanar bond angles θ of about 0.18 \AA and 119.4° , respectively. The Si_4B_2 trilayers present $a \approx 3.5 \text{ \AA}$, $\Delta z_{\text{Si-B}} \approx 0.09 \text{ \AA}$, and $\theta \approx 119.8^\circ$. As a result, those nanosheets doped with group-III atoms present low-buckled surfaces, as expected for sp^2 -type hybridiza-

tion in a Si host. In the trilayers functionalized with N or P atoms, the intraplanar bond angles θ and the intralayer $d_{\text{Si-X}}$ and buckling $\Delta z_{\text{Si-X}}$ distances show similar behavior to the functionalized bilayers doped with group-V atoms. Accordingly, those nanosheets present buckled surfaces.

Regarding AA'A''-Si₄Al₂ and ABC-Si₄Al₂ systems, the intralayer distances are, respectively, $d_{\text{Si-Al}} = 2.390$ and 2.399 Å, which are slightly smaller than the values found for the Si₂Al₂ bilayers. Although the Si-Si intralayer distance $d_{\text{Si-Si}}$ of around 2.52 Å is larger than the one in pure silicene trilayer (2.355 Å), silicon bulk (2.352 Å), or silicene monolayer (2.285 Å), the bond distance is still smaller than the longest Si-Si σ bonds (2.697 and $2.7288(15)$ Å).⁴¹ These systems also present a small variation of the buckling $\Delta z_{\text{Si-Si}}$ distances, with values of 0.802 Å for AA'A''-Si₄Al₂ and 0.782 Å for ABC-Si₄Al₂. Additionally, the $h_{\text{Si-Si}}$ distance between layers, i.e., the Si-Si interlayer distance, is similar to that in pristine silicene trilayers (2.423 and 2.435 Å) and close to the value of 2.365 Å obtained for the hydrogenated silicene,¹² showing that the Al incorporation does not disrupt the strong covalent Si-Si interactions.

As in the Si₄Al₂ systems, the functionalized Si₄B₂, Si₄N₂, and Si₄P₂ trilayers have strong Si-Si covalent bonds, presenting $h_{\text{Si-Si}}$ interlayer distance values close to the one in pristine silicene trilayers. Moreover, except for the Si₄N₂ system, these structures present Si-Si intralayer distances close to the value in pure silicene monolayer of 2.285 Å, being 2.272 and 2.282 Å for ABC- and AA'A''-Si₄B₂ systems, respectively, while they are 2.292 and 2.283 Å for ABC- and AA'A''-Si₄P₂ systems. In contrary, the $d_{\text{Si-Si}} = 2.807$ Å found for ABC-Si₄N₂ trilayer is larger than the longest known Si-Si σ bonds.⁴¹

The buckling Si-Si distance $\Delta z_{\text{Si-Si}}$ of 0.756 Å and 0.764 Å for pristine silicene trilayers in the AA'A and ABC stacking configurations, respectively, are very close to the Si bulk value of 0.784 Å. For the trilayer doped with Al, this buckling distance does not increase more than 6%, depending on the stacking configuration, when compared with pristine silicene. For the Si₄P₂ trilayers, regardless the stacking configuration, the $\Delta z_{\text{Si-Si}}$ distance increase is of about

17%, of the same magnitude observed for the Si_4B_2 system in the ABC stacking, which, however, is strongly affected, increasing by more than 34% when the stacking is AA'A". On the other hand, the N atom substitution causes huge modifications in the pristine Si-Si buckling distances, i.e., $\Delta z_{\text{Si-Si}}$ increases about 150% for AA'A"- Si_4N_2 stacking arrangement and has its value practically tripled for ABC stacking configuration. Those major changes have important implications on the system's dynamic stability, as will be discussed later.

Enthalpy of formation

We now discuss the possibility of synthesizing the Si_2X_2 and Si_4X_2 nanosheets, by analysing the values of the standard enthalpy of formation ΔH_f^0 , obtained by using Eq. 2 and comparing with the values for pristine silicene structures and graphene, the most well known 2D material. The values are shown in table 1.

A negative value of the enthalpy of formation indicates that the formation of a certain compound is exothermic, i.e., the amount of energy it takes to break bonds of the originating species is smaller than the amount of energy released when making the bonds. Herein, a negative ΔH_f^0 indicates the systems are stable or metastable, since $\Delta H_f^0 < 0$ is a necessary but not sufficient condition for thermodynamic stability.³⁷ Nevertheless, it is still possible to synthesize 2D materials by endothermic processes, i.e., with positive ΔH_f^0 . For instance, the ΔH_f^0 values of silicene and graphene monolayers are 751 meV/atom and 70 meV/atom,⁴² respectively. The ΔH_f^0 value of silicene obtained here is in good agreement with the available results reported in the literature.^{37,43}

It can be observed in table 1 that the calculated ΔH_f^0 values for pure silicene AA'- Si_4 and AB- Si_4 bilayers are 609 and 570 meV/atom, respectively, while they are 224 and 220 meV/atom for the AA'A- Si_6 and ABC- Si_6 trilayers, respectively. These results confirm the assertion that the FLS synthesis is easier than the silicene monolayer one. Particularly, it has been proposed that it is easier to experimentally produce free-standing 2D materials when the ΔH_f^0 is under the threshold energy value of 200 meV/atom.^{37,44,45}

Among the structures investigated, we found that the silicene bilayer and trilayer sheets doped with substitutional N or P atoms have negative ΔH_f^0 , where the exothermic reaction is likely due to the high reactivity of the silicene surface.¹⁰ The remaining systems have positive ΔH_f^0 , with values ranging between the threshold (200 meV/atom) and the silicene monolayer enthalpy of formation (751 meV/atom) energies.

Regarding the Si_2N_2 and Si_2P_2 bilayers, whose formation are exothermic, the AA' phase is slightly more favorable than the AB one. It is worth mentioning that the ΔH_f^0 results for Si_2P_2 are consistent with other results reported in the literature.⁴⁶ The Si_2B_2 bilayers are the least energetically favorable systems since they present the largest ΔH_f^0 values of 648 and 704 meV/atom for AA' and AB stacking, respectively, which is higher than the value found for pristine silicene bilayers. Oppositely, the Si_2Al_2 sheets are energetically more favorable than pure silicene bilayers since we found smaller ΔH_f^0 values of 446 and 404 meV/atom for the AA' and AB stacking configurations.

The doped silicene trilayers present a similar behavior as the bilayers: while the Si_4B_2 systems present the highest positive ΔH_f^0 among all Si_4X_2 structures, the Si_4N_2 exhibit the lowest negative ΔH_f^0 ones. Besides, the silicene trilayers doped with B or Al atoms are energetically less favorable than the pristine silicene trilayers, while the P doped ones present negative ΔH_f^0 values.

Dynamic stability and elasticity

To establish the structures' dynamic stability, we used the phonon theory to obtain the respective vibrational spectra. A certain structure is dynamically stable when it has only positive frequencies in the respective phonon dispersion curves. Table 1 presents the stability of all structures investigated here based on that criteria (DS). According to the table, silicene bilayers and trilayers functionalized with P atoms are dynamically stable. On the other hand, silicene structures functionalized with B, Al, or N are dynamically stable only in some stacking configurations.

The structures' phonon dispersion curves are presented in Fig. 2. Both stacking configurations of Si_2B_2 and Si_2Al_2 bilayers (Fig. 2(a), (b), (c), and (d)) and of Si_4N_2 trilayers (Fig. 2(m) and (n)), as well as the $\text{AA}'\text{A}''\text{-Si}_4\text{B}_2$ system (Fig. 2(i)) and $\text{AA}'\text{A}''\text{-Si}_4\text{Al}_2$ trilayer (Fig. 2(k)), present large negative frequencies and, hence, they are dynamically unstable. Moreover, the small negative frequency around the Γ valley in the $\text{ABC-Si}_4\text{B}_2$ system, shown in Fig. 2(j), could indicate that this sheet has lower stability than the other dynamically stable trilayers studied here. This behavior has been found in some theoretical investigations of 2D materials, and has been generally associated with the difficulty in converging the out-of-plane ZA transverse acoustic mode.^{17,47}

We computed the elastic constants of the systems with Eq. 1, which must satisfy $C_{11} > 0$ and $C_{12} < C_{11}$ for elastic stability (Born stability criteria).⁴⁸ Moreover, for the dynamically stable (DS) bilayers and trilayers presented in table 1, we also evaluated the C_{44} elastic constant through $C_{44} = (C_{11} - C_{12})/2$ expression, the Young modulus $Y^{2\text{D}} = (C_{11}^2 - C_{12}^2)/C_{11}$, and the Poisson ratio $\nu = C_{12}/C_{11}$. The results are displayed in table 2, which confirm what was observed in the phonon dispersion spectra shown in figure 2, regarding the stability of the compounds, once all the dynamically stable systems satisfy the Born criteria. For the pristine silicene monolayer, the calculated values for all the elastic constants are in concordance with data from the literature.¹⁰ Moreover, the C_{11} elastic constant of the pure AB-Si_4 bilayer of 121 N/m and ABC-Si_6 trilayer of 167 N/m are also in agreement with previously reported results.³⁸

Additionally, we observe that pristine FLS structures are more stable as they grow in thickness, i.e., the elastic constants and the $Y^{2\text{D}}$ increase with the number of layers.³⁸ For the functionalized FLS, the $Y^{2\text{D}}$ values range from 66 to 273 N/m, which are directly related to the systems' lattice parameter a and intralayer distances d . The Si_2N_2 bilayers have the smallest a and the largest $Y^{2\text{D}}$, while the $\text{ABC-Si}_4\text{Al}_2$ trilayer has the largest a and the lowest $Y^{2\text{D}}$. The remaining systems follow the same trend, which has also been observed in other 2D systems.³⁹ Furthermore, except for the $\text{ABC-Si}_4\text{Al}_2$, all the systems investigated

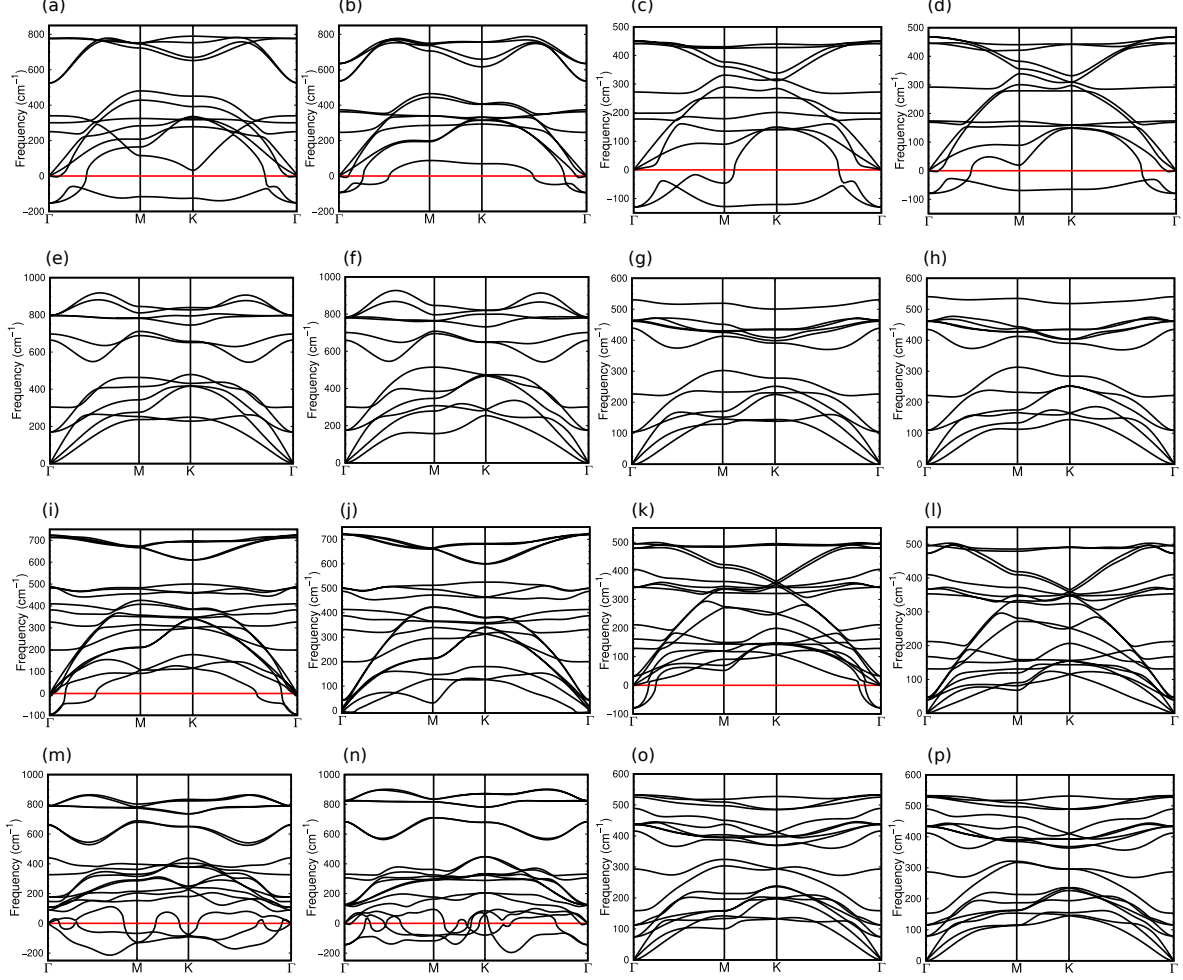


Figure 2: Phonon dispersion curves along the main high symmetry directions of the irreducible Brillouin zone (BZ) of the hexagonal lattice: (a) AA'-Si₂B₂, (b) AB-Si₂B₂, (c) AA'-Si₂Al₂, (d) AB-Si₂Al₂, (e) AA'-Si₂N₂, (f) AB-Si₂N₂, (g) AA'-Si₂P₂, (h) AB-Si₂P₂, (i) AA'A''-Si₄B₂, (j) ABC-Si₄B₂, (k) AA'A''-Si₄Al₂, (l) ABC-Si₄Al₂, (m) AA'A''-Si₄N₂, (n) ABC-Si₄N₂, (o) AA'A''-Si₄P₂, and (p) ABC-Si₄P₂.

have Poisson ratio ν between 0.17 and 0.30, in the 0-0.5 range which has been observed in 2D materials³⁹ and isotropic systems.⁴⁹ Although the ν value of 0.68 obtained for the ABC-Si₄Al₂ trilayer is larger than 0.5, it is similar to values found in stretched silicene monolayer of 0.62⁵⁰ and 0.75.⁵¹ Indeed, the Al atom substitution in pristine silicene trilayer increases the lattice parameter and, hence, the Si-Si bond distances.

Our results show that the stability of the binary bilayers depends on the X atoms, as we find that the combination between group-V and group-IV elements, as in Si₂N₂ and Si₂P₂ structures, produces dynamically stable systems as they exhibit only positive frequencies

Table 2: Elastic constants C_{11} , C_{12} , and C_{44} , Young’s modulus Y^{2D} , and Poisson ratio ν of pristine FLS, Si_2X_2 , and Si_4X_2 ($\text{X} = \text{B}, \text{N}, \text{Al}, \text{P}$) for the dynamically stable configurations. Elastic constants and Young’s modulus are given in N/m and Poisson ratio is dimensionless.

System	Structure	Stacking	C_{11}	C_{12}	C_{44}	Y^{2D}	ν
Monolayer	Si_2	—	69	19	25	64	0.28
	Si_4	AA'	124	36	44	113	0.29
AB		121	33	43	111	0.28	
Bilayer	Si_2N_2	AA'	296	83	106	273	0.28
		AB	278	83	97	252	0.30
	Si_2P_2	AA'	133	24	55	129	0.18
		AB	129	23	53	125	0.18
Trilayer	Si_6	AA'A	157	33	62	150	0.21
		ABC	167	43	62	156	0.25
	Si_4B_2	ABC	198	35	82	192	0.17
	Si_4Al_2	ABC	123	84	20	66	0.68
	Si_4P_2	AA'A''	182	38	72	174	0.21
		ABC	176	36	70	168	0.21

and satisfy the Born stability criteria. On the other hand, there is no dynamic stability for the compounds that involve combinations of group-III and group-IV elements, i.e., Si_2B_2 and Si_2Al_2 bilayers.

In the trilayers, the stable systems are $\text{ABC-Si}_4\text{B}_2$, $\text{ABC-Si}_4\text{Al}_2$, $\text{AA'A''-Si}_4\text{P}_2$, and $\text{ABC-Si}_4\text{P}_2$, in which the higher structural stability is related to the system with shorter interlayer distances $h_{\text{Si-Si}}$, which leads to the strong interactions between layers.¹² The instability in the $\text{ABC-Si}_4\text{N}_2$ compound is likely associated with the large Si-Si intralayer bond distance $d_{\text{Si-Si}}$ of 2.807 Å and the huge buckling distance $\Delta z_{\text{Si-Si}}$ of 2.267 Å in the non-doped intermediate silicene layer. The $d_{\text{Si-Si}}$ is larger than the longest Si-Si σ bonds (2.697 and 2.7288(15) Å)⁴¹ and the huge $\Delta z_{\text{Si-Si}}$ is related to the multilayer silicene instability.¹¹ As in the $\text{ABC-Si}_4\text{N}_2$ system, the instability of the $\text{AA'A''-Si}_4\text{N}_2$ is also due to the large Si-Si intralayer bond distance $d_{\text{Si-Si}} = 2.508$ Å and the huge buckling distance $\Delta z_{\text{Si-Si}} = 1.861$

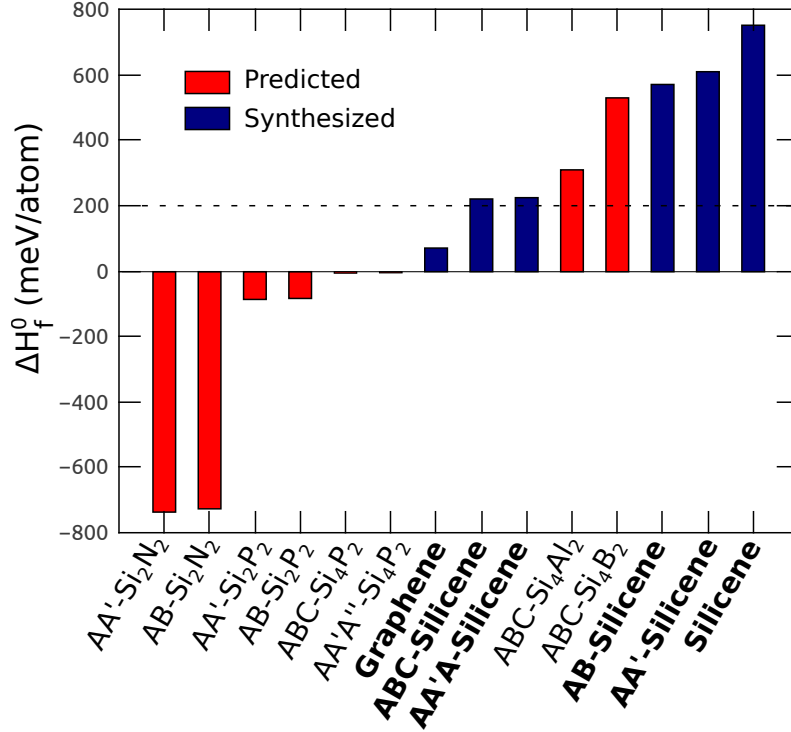


Figure 3: Standard enthalpy of formation, calculated using Eq. 2, for the dynamically stable systems. The horizontal dashed line illustrates the empirical threshold energy to experimentally synthesize free-standing 2D materials.^{37,44,45}

Å. Regarding the AA'A''-Si₄B₂ and AA'A''-Si₄Al₂ structures, they present similar behavior since there is a huge negative frequency around the Γ valley, suggesting that a possible synthesis of Si₄B₂ and Si₄Al₂ trilayers should be in the ABC stacking configuration.

Figure 3 shows the standard enthalpy of formation for all the dynamically stable structures found here. The empirical threshold energy (200 meV/atom) to experimentally synthesize free-standing 2D materials^{37,44,45} is also shown. Although FLS has enthalpies of formation greater than 200 meV, they have been free-standing synthesized.¹⁵ The graphene enthalpy of formation is also included for comparison, which was computed, with respect to graphite, computed using the van der Waals density functional (optB88-vdW) to describe the exchange-correlation energy.⁴² The comparison shows the feasibility of experimentally synthesizing, through different techniques, the dynamically stable systems investigated here.

Electronic properties

Figures 4 and 5 display the electronic band structures and the projected density of states (PDOS) of the dynamically stable Si_2X_2 and Si_4X_2 systems ($\text{X} = \text{B}, \text{N}, \text{Al}, \text{P}$), as well as the ones of the pristine silicene monolayer Si_2 , bilayers Si_4 , and trilayers Si_6 . Table 3 presents the systems' classification and list the values of the indirect electronic band gaps E_g , the high-symmetry point or direction of the valence band maximum (VBM) and conduction band minimum (CBM), and their atomic character.

Previous studies have shown that pure silicene monolayer has zero band gap with a Dirac cone at the K-point in the Brillouin zone⁴ and FLS can present metallic or semiconducting behavior depending on the stacking configuration.^{11,13,14} All of our results for pristine silicene structures, displayed in Fig. 4(a) for Si_2 , Fig. 4(b) and (c) for Si_4 , and Fig. 5(a) and (b) for Si_6 , agree well with the ones reported in the literature, where the investigated FLS are metallic structures. For the functionalized FLS, we found that the $\text{AA}'\text{-Si}_2\text{N}_2$, $\text{AB-Si}_2\text{N}_2$, $\text{AA}'\text{-Si}_2\text{P}_2$, and $\text{AB-Si}_2\text{P}_2$ doped bilayers, Fig. 4 (d)-(g), and the $\text{AA}'\text{A}''\text{-Si}_4\text{P}_2$ and $\text{ABC-Si}_4\text{P}_2$ doped trilayers, Fig. 5(e) and (f), are indirect band gap semiconductors, while the $\text{ABC-Si}_4\text{B}_2$ and $\text{ABC-Si}_4\text{Al}_2$ trilayers, Fig. 5(c) and (d), are metallic. It should be noticed that these band gap values should be considered as lower limits, as the DFT/vdW is known to underestimate them.

The differences in the electronic properties result from the distinct X doping elements that composed the systems, i.e., the prevailing factor that determined the properties of the compounds is the number of valence electrons of the X atoms. The group-V atoms (N, P) substitution transforms the pristine silicene bilayers and trilayers from metallic to semiconductor. In contrast, the B or Al substitution keeps the metallic behavior of pristine silicene trilayers. Additionally, the Dirac cone in the metallic pristine silicene trilayers, which is below the Fermi energy at the K-point for $\text{AA}'\text{A}$ stacking configuration, Fig. 5(a), and in the K-M direction for ABC one, Fig. 5(b),¹¹ is not preserved in the Si_4X_2 systems. The electronic band gaps (E_g) for $\text{AA}'\text{-Si}_2\text{N}_2$, $\text{AB-Si}_2\text{N}_2$, $\text{AA}'\text{-Si}_2\text{P}_2$, $\text{AB-Si}_2\text{P}_2$, $\text{AA}'\text{A}''\text{-Si}_4\text{P}_2$,

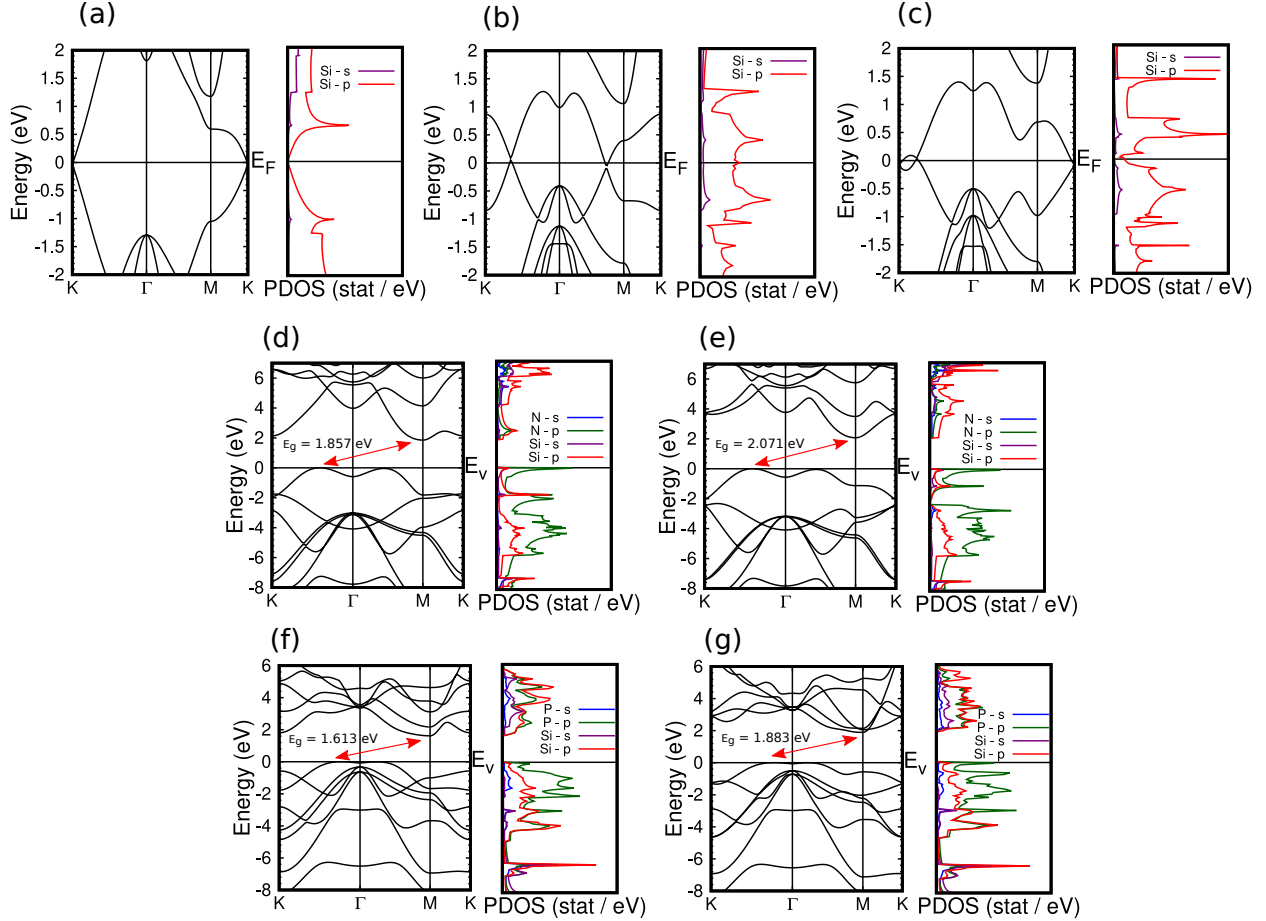


Figure 4: Electronic band structures along the main high-symmetry directions of the BZ (left panels) and projected density of states (PDOS) (right panels) of (a) Si_2 , (b) $\text{AA}'\text{-Si}_4$, (c) AB-Si_4 , (d) $\text{AA}'\text{-Si}_2\text{N}_2$, (e) $\text{AB-Si}_2\text{N}_2$, (f) $\text{AA}'\text{-Si}_2\text{P}_2$, and (g) $\text{AB-Si}_2\text{P}_2$. The PDOS, in units of number of states/eV, on the Si and X s -orbitals are given in purple and blue, respectively, and on the Si and X p -orbitals are given in red and green, respectively. E_V represents the valence band top and E_F the Fermi energy.

and $\text{ABC-Si}_4\text{P}_2$, are 1.857, 2.071, 1.613, 1.883, 0.898, and 1.007 eV, respectively. The E_g values of Si_2N_2 and Si_2P_2 functionalized bilayers are in good agreement with reported theoretical results that used the PBE functional approximation for the exchange-correlation energy, values that increased by up to 1 eV (Si_2N_2) and 0.7 eV (Si_2P_2) when the Heyd-Scuseria-Ernzerhof screen-exchange hybrid functional (HSE06) was used,¹⁶ suggesting that the electronic band gaps presented in table 3 are likely underestimated by at least 0.7 eV.

For the Si_2N_2 and Si_2P_2 semiconducting bilayers, Fig. 4 (d)-(g) show that the bottom of the conduction band, at M-point, and the top of the valence band, at the high-symmetry

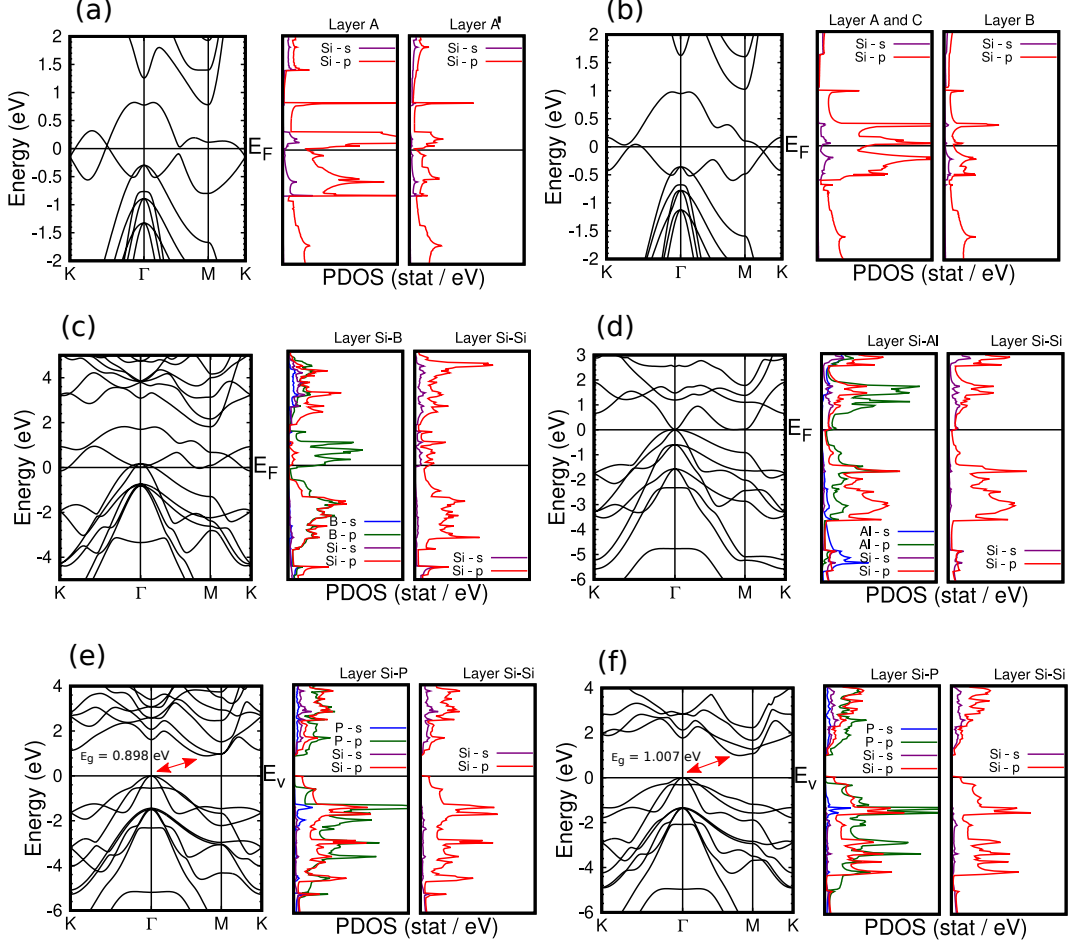


Figure 5: Electronic band structures along the main high-symmetry directions of the BZ (left panels) and projected density of states (PDOS) (right panels) of (a) $AA'A-Si_6$, (b) $ABC-Si_6$, (c) $ABC-Si_4B_2$, (d) $ABC-Si_4Al_2$, (e) $AA'A''-Si_4P_2$, and (f) $ABC-Si_4P_2$. The PDOS, in units of number of states/eV, on the Si and X s -orbitals are given in purple and blue, respectively, and on the Si and X p -orbitals are given in red and green, respectively. E_v represents the valence band top and E_F the Fermi energy.

$K-\Gamma$ direction, have contributions mainly from the hybridization of the Si and X p -states ($X = N, P$), with prevailing X p -states character. Moreover, the top region of the valence band is highly degenerated with a Mexican-hat dispersion (quartic function), in accordance with other investigations.¹⁶

The $AA'A''-Si_4P_2$ and $ABC-Si_4P_2$ semiconducting trilayers have similar band structures and PDOS, as shown in Fig. 5 (e) and (f), with the VBM at the Γ -point and the CBM at the Γ -M direction. The PDOS shows that the Si p -orbitals derived from the intermediate

Table 3: Electronic properties of the pristine and doped FLS, for the dynamically stable configurations: indirect electronic band gaps $E_g(i)$, given in eV, valence band maximum (VBM) and conduction band minimum (CBM) high-symmetry point or direction (hexagonal BZ), and the atomic character of VBM and CBM. These parameters were obtained using the optB88-vdW approximation to describe the exchange-correlation energy. The systems with metallic behavior are also shown.

System	Structure	Stacking	Classification	$E_g(i)$	VBM (character)	CBM (character)
Monolayer	Si ₂	—	semimetal	0	—	—
Bilayer	Si ₄	AA'	metal	—	—	—
		AB	metal	—	—	—
	Si ₂ N ₂	AA'	semiconductor	1.857	K- Γ (Si- p , N- p)	M (Si- p , N- p)
		AB	semiconductor	2.071	K- Γ (Si- p , N- p)	M (Si- p)
Si ₂ P ₂	AA'	semiconductor	1.613	K- Γ (Si- p , P- p)	M (Si- p , P- p)	
	AB	semiconductor	1.883	K- Γ (Si- p , P- p)	M (Si- p , P- p)	
Trilayer	Si ₆	AA'A	metal	—	—	—
		ABC	metal	—	—	—
	Si ₄ B ₂	ABC	metal	—	—	—
	Si ₄ Al ₂	ABC	metal	—	—	—
Si ₄ P ₂	AA'A''	semiconductor	0.898	Γ (Si- p)	Γ -M (Si- p , P- p)	
	ABC	semiconductor	1.007	Γ (Si- p)	Γ -M (Si- p , P- p)	

(non-doped) Si-Si layer and from the Si-P layer dominate at the VBM, while at the CBM there is also a contribution of the P p -states from the Si-P layer. In the ABC–Si₄B₂ and ABC–Si₄Al₂ metallic systems, Fig. 5 (c) and (d), the Fermi level crosses three bands, in the Γ -point region, that have contributions from the hybridization of the Si and X p -orbitals of the Si-X layer (X = B, Al), and from the Si s -state of the Si-Si layer. Moreover, the Fermi level crossing around the K-point in the ABC–Si₄B₂ is mainly derived from the B p -states of the Si-B layer and from Si p -states of the Si-Si layer.

These results provide chemical routes to tune and control the FLS electronic structure by increasing the number of layers and, at the same time, doping them to be used in specific applications.

Discussion and Concluding Remarks

In summary, we performed a theoretical investigation on the structural, energetic, dynamic, elastic, and electronic properties of silicene bilayers and trilayers functionalized with group-III and group-V atoms in several stacking configurations. We identified a number of functionalized FLS that are dynamically stable and experimentally accessible, based on the results of the enthalpies of formation, phonon dispersion spectra, and Born stability criteria. Additionally, among them we found that two structures present metallic behavior while the others present semiconducting properties, accordingly to the respective electronic structures, which are directly associated with the atomic species used in the functionalization.

The ABC-Si₄B₂ and ABC-Si₄Al₂ metallic systems present low-buckled surfaces, being the least favorable of the structures studied since they have the greatest positive enthalpy of formation. However, the enthalpies of formation of these systems are still lower than that of pristine silicene monolayer, which has already been synthesized. In particular, the AA'A''-Si₄P₂ and ABC-Si₄P₂ semiconductor trilayers present an enthalpy of formation nearly zero, i.e., which is lower than the empirical threshold energy of 200 meV/atom for the synthesis of free-standing 2D materials and, therefore, considering the recent synthesis of several 2D materials, the structures studied here are likely to be produced in a near future.

Further investigations could explore the applicability of the structures propose here. Previous studies have shown that functionalized nanostructures could serve as building blocks for the self-assembly of complex 3D systems.^{2,42,52} Particularly, 2D building blocks could be vertically combined to make 2D/3D systems with tailored properties.^{2,42} Recently, van der Waals heterostructures based on silicon SiX (X = N, P, As, Sb, Bi) have been investigated in several stacking configurations, in which the SiN was proposed for water oxidation applications and the SiP for photocatalytic water splitting.⁵³ Therefore, considering the silicon-based structures investigated here, it is interesting to explore if those systems could be used as building blocks and how their properties would modify with different morphologies. The Si₂N₂ and Si₂P₂ bilayers have been considered for UV-light applications due to

their wide band gap¹⁶ and as thermoelectric materials at room temperature.⁵⁴ Within such context, the AA'A''-Si₄P₂ and ABC-Si₄P₂ nanosheets could be explored as thermoelectric materials. Although we found a narrower band gap for these systems in comparison with Si₂P₂ bilayers, it is important once more emphasizing that the band gap is here underestimated due to the DFT/vdW approximation and, hence, we suggest the AA'A''-Si₄P₂ and ABC-Si₄P₂ semiconducting trilayers could be appropriated for UV-light application as well.

Moreover, silicene monolayer and FLS nanosheets are promising candidates for energy storage system applications, such as lithium-ion batteries.^{15,55} Peculiarly, the silicene monolayer doped with different elements has shown good performance for alkali metal ion batteries (AMIBs). For instance, B/Al doped silicene has low diffusion barriers and higher capacity for sodium-ion batteries (SIBs) and potassium-ion batteries (KIBs) in comparison to pristine silicene.⁵⁶ Therefore, since good electrical conductivity is one of the requirements for advanced electrodes,⁵⁷ the ABC-Si₄B₂ and ABC-Si₄Al₂ metallic structures are promising candidates for AMIBs applications.

Acknowledgement

This investigation was partially supported by Brazilian federal government agencies CAPES and CNPq. The authors acknowledge the National Laboratory for Scientific Computing (LNCC/MCTI, Brazil) for providing HPC resources of the Santos Dumont supercomputer (<http://sdumont.lncc.br>) and Centro Nacional de Processamento de Alto Desempenho em São Paulo (CENAPAD-SP, Brazil). LVCA and JFJ acknowledge support from Brazilian agency CNPq, under projects numbers 305753/2017-7 and 305187/2018-0.

References

- (1) Novoselov, K. S.; Geim, A. K.; Morozov, S. V.; Jiang, D.; Zhang, Y.; Dubonos, S. V.; Grigorieva, I. V.; Firsov, A. A. Electric field effect in atomically thin carbon films.

- Science* **2004**, *306*, 666–669.
- (2) Novoselov, K. S.; Mishchenko, A.; Carvalho, A.; Castro Neto, A. H. 2D materials and van der Waals heterostructures. *Science* **2016**, *353*, aac9439.
 - (3) Li, G.; Zhang, Y.-Y.; Guo, H.; Huang, L.; Lu, H.; Lin, X.; Wang, Y.-L.; Du, S.; Gao, H.-J. Epitaxial growth and physical properties of 2D materials beyond graphene: from monatomic materials to binary compounds. *Chemical Society Reviews* **2018**, *47*, 6073–6100.
 - (4) Cahangirov, S.; Topsakal, M.; Aktürk, E.; Şahin, H.; Ciraci, S. Two- and one-dimensional honeycomb structures of silicon and germanium. *Physical Review Letters* **2009**, *102*, 236804.
 - (5) Garcia, J. C.; de Lima, D. B.; Assali, L. V. C.; Justo, J. F. Group IV graphene- and graphane-like nanosheets. *The Journal of Physical Chemistry C* **2011**, *115*, 13242–13246.
 - (6) Schoop, L. M.; Pielhofer, F.; Lotsch, B. V. Chemical principles of topological semimetals. *Chemistry of Materials* **2018**, *30*, 3155–3176.
 - (7) Molle, A.; Grazianetti, C.; Tao, L.; Taneja, D.; Alam, M. H.; Akinwande, D. Silicene, silicene derivatives, and their device applications. *Chemical Society Reviews* **2018**, *47*, 6370–6387.
 - (8) Zhuang, J.; Xu, X.; Feng, H.; Li, Z.; Wang, X.; Du, Y. Honeycomb silicon: a review of silicene. *Science Bulletin* **2015**, *60*, 1551–1562.
 - (9) Sivek, J.; Sahin, H.; Partoens, B.; Peeters, F. M. Adsorption and absorption of boron, nitrogen, aluminum, and phosphorus on silicene: Stability and electronic and phonon properties. *Physical Review B* **2013**, *87*, 085444.

- (10) Ding, Y.; Wang, Y. Density functional theory study of the silicene-like SiX and XSi₃ (X= B, C, N, Al, P) honeycomb lattices: the various buckled structures and versatile electronic properties. *The Journal of Physical Chemistry C* **2013**, *117*, 18266–18278.
- (11) Qian, C.; Li, Z. Multilayer silicene: structure, electronics, and mechanical property. *Computational Materials Science* **2020**, *172*, 109354.
- (12) Liu, Y.; Shu, H.; Liang, P.; Cao, D.; Chen, X.; Lu, W. Structural, electronic, and optical properties of hydrogenated few-layer silicene: size and stacking effects. *Journal of Applied Physics* **2013**, *114*, 094308.
- (13) Padilha, J. E.; Pontes, R. B. Free-standing bilayer silicene: the effect of stacking order on the structural, electronic, and transport properties. *The Journal of Physical Chemistry C* **2015**, *119*, 3818–3825.
- (14) Fu, H.; Zhang, J.; Ding, Z.; Li, H.; Meng, S. Stacking-dependent electronic structure of bilayer silicene. *Applied Physics Letters* **2014**, *104*, 131904.
- (15) Liu, J.; Yang, Y.; Lyu, P.; Nachtigall, P.; Xu, Y. Few-layer silicene nanosheets with superior lithium-storage properties. *Advanced Materials* **2018**, *30*, 1800838.
- (16) Özdamar, B.; Özbal, G.; Çınar, M. N.; Sevim, K.; Kurt, G.; Kaya, B.; Sevinçli, H. Structural, vibrational, and electronic properties of single-layer hexagonal crystals of group IV and V elements. *Physical Review B* **2018**, *98*, 045431.
- (17) Touski, S. B.; Ghobadi, N. Structural, electrical, and Rashba properties of monolayer Janus Si₂XY (X, Y= P, As, Sb, and Bi). *Physical Review B* **2021**, *103*, 165404.
- (18) Yang, J.-H.; Zhang, Y.; Yin, W.-J.; Gong, X.; Yakobson, B. I.; Wei, S.-H. Two-dimensional SiS layers with promising electronic and optoelectronic properties: theoretical prediction. *Nano Letters* **2016**, *16*, 1110–1117.

- (19) An, Y.; Tian, Y.; Wei, C.; Zhang, Y.; Xiong, S.; Feng, J.; Qian, Y. Recent advances and perspectives of 2D silicon: synthesis and application for energy storage and conversion. *Energy Storage Materials* **2020**, *32*, 115–150.
- (20) Tantardini, C.; Kvashnin, A. G.; Gatti, C.; Yakobson, B. I.; Gonze, X. Computational modeling of 2D materials under high pressure and their chemical bonding: silicene as possible field-effect transistor. *ACS Nano* **2021**, *15*, 6861–6871.
- (21) Giannozzi, P.; Baroni, S.; Bonini, N.; Calandra, M.; Car, R.; Cavazzoni, C.; Ceresoli, D.; Chiarotti, G. L.; Cococcioni, M.; Dabo, I. *et al.* QUANTUM ESPRESSO: a modular and open-source software project for quantum simulations of materials. *Journal of physics: Condensed matter* **2009**, *21*, 395502.
- (22) Giannozzi, P.; Andreussi, O.; Brumme, T.; Bunau, O.; Nardelli, M. B.; Calandra, M.; Car, R.; Cavazzoni, C.; Ceresoli, D.; Cococcioni, M. *et al.* Advanced capabilities for materials modelling with Quantum ESPRESSO. *Journal of Physics: Condensed Matter* **2017**, *29*, 465901.
- (23) Hohenberg, P.; Kohn, W. Inhomogeneous electron gas. *Physical Review* **1964**, *136*, B864.
- (24) Kohn, W.; Sham, L. J. Self-consistent equations including exchange and correlation effects. *Physical Review* **1965**, *140*, A1133.
- (25) Kresse, G.; Joubert, D. From ultrasoft pseudopotentials to the projector augmented-wave method. *Physical Review B* **1999**, *59*, 1758–1775.
- (26) Perdew, J. P.; Burke, K.; Ernzerhof, M. Generalized gradient approximation made simple. *Physical Review Letters* **1996**, *77*, 3865.
- (27) Dion, M.; Rydberg, H.; Schröder, E.; Langreth, D. C.; Lundqvist, B. I. Van der Waals density functional for general geometries. *Physical Review Letters* **2004**, *92*, 246401.

- (28) Klimeš, J.; Bowler, D. R.; Michaelides, A. Chemical accuracy for the van der Waals density functional. *Journal of Physics: Condensed Matter* **2009**, *22*, 022201.
- (29) Zhang, G.-X.; Tkatchenko, A.; Paier, J.; Appel, H.; Scheffler, M. Van der Waals interactions in ionic and semiconductor solids. *Physical Review Letters* **2011**, *107*, 245501.
- (30) Park, J.; Yu, B. D.; Hong, S. Van der Waals density functional theory study for bulk solids with BCC, FCC, and diamond structures. *Current Applied Physics* **2015**, *15*, 885–891.
- (31) Marcondes, M. L.; Wentzcovitch, R. M.; Assali, L. V. C. Importance of van der Waals interaction on structural, vibrational, and thermodynamic properties of NaCl. *Solid State Communications* **2018**, *273*, 11–16.
- (32) Monkhorst, H. J.; Pack, J. D. Special points for Brillouin-zone integrations. *Physical Review B* **1976**, *13*, 5188–5192.
- (33) Baroni, S.; De Gironcoli, S.; Dal Corso, A.; Giannozzi, P. Phonons and related crystal properties from density-functional perturbation theory. *Reviews of Modern Physics* **2001**, *73*, 515–562.
- (34) Cadelano, E.; Palla, P. L.; Giordano, S.; Colombo, L. Elastic properties of hydrogenated graphene. *Physical Review B* **2010**, *82*, 235414.
- (35) Assali, L. V. C.; Machado, W. V. M.; Justo, J. F. Manganese impurities in boron nitride. *Applied Physics Letters* **2006**, *89*, 072102.
- (36) Assali, L. V. C.; Machado, W. V. M.; Justo, J. F. 3d transition metal impurities in diamond: electronic properties and chemical trends. *Physical Review B* **2011**, *84*, 155205.
- (37) Hastrup, S.; Strange, M.; Pandey, M.; Deilmann, T.; Schmidt, P. S.; Hinsche, N. F.; Gjerding, M. N.; Torelli, D.; Larsen, P. M.; Riis-Jensen, A. C. *et al.* The computational

- 2D materials database: high-throughput modeling and discovery of atomically thin crystals. *2D Materials* **2018**, *5*, 042002.
- (38) Li, Y.; Tang, G.; Fu, B. Hydrogenation: an effective strategy to improve the thermoelectric properties of multilayer silicene. *Physical Review B* **2019**, *99*, 235428.
- (39) Hess, P. Bonding, structure, and mechanical stability of 2D materials: the predictive power of the periodic table. *Nanoscale Horizons* **2021**, *6*, 856–892.
- (40) Kamal, C.; Chakrabarti, A.; Banerjee, A.; Deb, S. Silicene beyond mono-layers – different stacking configurations and their properties. *Journal of Physics: Condensed Matter* **2013**, *25*, 085508.
- (41) Kyushin, S.; Kurosaki, Y.; Otsuka, K.; Imai, H.; Ishida, S.; Kyomen, T.; Hanaya, M.; Matsumoto, H. Silicon–silicon π single bond. *Nature Communications* **2020**, *11*, 1–7.
- (42) Ipaves, B.; Justo, J. F.; Assali, L. V. C. Carbon-related bilayers: nanoscale building blocks for self-assembly nanomanufacturing. *The Journal of Physical Chemistry C* **2019**, *123*, 23195–23204.
- (43) Revard, B. C.; Tipton, W. W.; Yesypenko, A.; Hennig, R. G. Grand-canonical evolutionary algorithm for the prediction of two-dimensional materials. *Physical Review B* **2016**, *93*, 054117.
- (44) Ashton, M.; Sinnott, S. B.; Hennig, R. G. Computational discovery and characterization of polymorphic two-dimensional IV–V materials. *Applied Physics Letters* **2016**, *109*, 192103.
- (45) Gjerding, M.; Taghizadeh, A.; Rasmussen, A.; Ali, S.; Bertoldo, F.; Deilmann, T.; Holguin, U.; Knøsgaard, N.; Kruse, M.; Manti, S. *et al.* Recent progress of the computational 2D materials database (C2DB). *2D Materials* **2021**, *8*, 044002.

- (46) Huang, B.; Zhuang, H. L.; Yoon, M.; Sumpter, B. G.; Wei, S.-H. Highly stable two-dimensional silicon phosphides: different stoichiometries and exotic electronic properties. *Physical Review B* **2015**, *91*, 121401.
- (47) Mohebpour, M. A.; Mozvashi, S. M.; Vishkayi, S. I.; Tagani, M. B. Prediction of hydrogenated group IV–V hexagonal binary monolayers. *Scientific Reports* **2020**, *10*, 1–14.
- (48) Mouhat, F.; Coudert, F.-X. Necessary and sufficient elastic stability conditions in various crystal systems. *Physical Review B* **2014**, *90*, 224104.
- (49) Gercek, H. Poisson’s ratio values for rocks. *International Journal of Rock Mechanics and Mining Sciences* **2007**, *44*, 1–13.
- (50) Wang, B.; Wu, J.; Gu, X.; Yin, H.; Wei, Y.; Yang, R.; Dresselhaus, M. Stable planar single-layer hexagonal silicene under tensile strain and its anomalous Poisson’s ratio. *Applied Physics Letters* **2014**, *104*, 081902.
- (51) Das, D.; Sarkar, J. Comparison of mechanical properties of silicene estimated using different testing procedures: a molecular dynamics study. *Journal of Applied Physics* **2018**, *123*, 044304.
- (52) Garcia, J. C.; Justo, J. F.; Machado, W. V. M.; Assali, L. V. C. Functionalized adamantane: building blocks for nanostructure self-assembly. *Physical Review B* **2009**, *80*, 125421.
- (53) Somaiya, R.; Singh, D.; Sonvane, Y. K.; Gupta, S. K.; Ahuja, R. Potential SiX (X= N, P, As, Sb, Bi) homo-bilayers for visible-light photocatalysts application. *Catalysis Science & Technology* **2021**, *11*, 4996–5013.
- (54) Somaiya, R. N.; Sonvane, Y. A.; Gupta, S. K. Exploration of the strain and thermoelectric properties of hexagonal SiX (X= N, P, As, Sb, and Bi) monolayers. *Physical Chemistry Chemical Physics* **2020**, *22*, 3990–3998.

- (55) Zhuang, J.; Xu, X.; Peleckis, G.; Hao, W.; Dou, S. X.; Du, Y. Silicene: a promising anode for lithium-ion batteries. *Advanced Materials* **2017**, *29*, 1606716.
- (56) Zhu, J.; Gandi, A. N.; Schwingenschlögl, U. Potential of B/Al-doped silicene electrodes in Na/K-ion batteries. *Advanced Theory and Simulations* **2018**, *1*, 1800017.
- (57) Zhang, C.; Wang, F.; Han, J.; Bai, S.; Tan, J.; Liu, J.; Li, F. Challenges and recent progress on silicon-based anode materials for next-generation lithium-ion batteries. *Small Structures* **2021**, *6*, 2170015.

Graphical TOC Entry

